Structure and Mechanism of an ADP-Glucose Phosphorylase from *Arabidopsis thaliana*[†,‡]

Jason G. McCoy,[§,||] Abolfazl Arabshahi,[§] Eduard Bitto,[||] Craig A. Bingman,[||] Frank J. Ruzicka,[§] Perry A. Frey,[§] and George N. Phillips, Jr.*[,§,||]

Department of Biochemistry, University of Wisconsin, Madison, Wisconsin 53706, and University of Wisconsin Center for Eukaryotic Structural Genomics, University of Wisconsin, Madison, Wisconsin 53706

Received November 1, 2005; Revised Manuscript Received January 19, 2006

ABSTRACT: The X-ray crystal structure of the At5g18200.1 protein has been determined to a nominal resolution of 2.30 Å. The structure has a histidine triad (HIT)-like fold containing two distinct HIT-like motifs. The sequence of At5g18200.1 indicates a distant family relationship to the *Escherichia coli* galactose-1-P uridylyltransferase (GalT): the determined structure of the At5g18200.1 protein confirms this relationship. The At5g18200.1 protein does not demonstrate GalT activity but instead catalyzes adenylyl transfer in the reaction of ADP-glucose with various phosphates. The best acceptor among those evaluated is phosphate itself; thus, the At5g18200.1 enzyme appears to be an ADP-glucose phosphorylase. The enzyme catalyzes the exchange of ^{14}C between ADP-[^{14}C]glucose and glucose-1-P in the absence of phosphate. The steady state kinetics of exchange follows the ping-pong bi-bi kinetic mechanism, with a k_{cat} of 4.1 s^{-1} and K_m values of 1.4 and 83 μM for ADP-[^{14}C]glucose and glucose-1-P, respectively, at pH 8.5 and 25 °C. The overall reaction of ADP-glucose with phosphate to produce ADP and glucose-1-P follows ping-pong bi-bi steady state kinetics, with a k_{cat} of 2.7 s^{-1} and K_m values of 6.9 and 90 μM for ADP-glucose and phosphate, respectively, at pH 8.5 and 25 °C. The kinetics are consistent with a double-displacement mechanism that involves a covalent adenylyl−enzyme intermediate. The X-ray crystal structure of this intermediate was determined to 1.83 Å resolution and shows the AMP group bonded to His^{186}. The value of K_{eq} in the direction of ADP and glucose-1-P formation is 5.0 at pH 7.0 and 25 °C in the absence of a divalent metal ion, and it is 40 in the presence of 1 mM $MgCl_2$.

The At5g18200.1 sequence belongs to the histidine triad (HIT)[1] superfamily of nucleotide hydrolases and transferases (superfamily E = 3.0e-45 and 1.0e-29 for the C- and N-terminal portions, respectively) (*1*). This superfamily contains three distinct families: the histidine triad nucleotide-binding protein family, the fragile histidine triad family, and the GalT family (*2*). The At5g18200.1 enzyme is a member of the GalT family, which differs from the other two families in several respects: it does not contain a "triad of histidines" but rather a conserved HXHXQ sequence, and the typical reaction catalyzed by enzymes of this family is nucleotidyl transfer rather than hydrolysis (*3*). The GalT family contains three known subfamilies of enzymes (*3*): the GALT-like UDP-hexose:hexose-1-P uridylyltransferases, an adenylylsulfate:phosphate adenylyltransferase from *Thiobacillus denitrificans* which converts adenosine 5′-phosphosulfate and phosphate to ADP and sulfate (*4*), and diadenosine tetraphosphate phosphorylase whose catalytic activity results in the formation of ATP and ADP (*5*).

In the genome of *Arabidopsis thaliana*, the locus At5g18200.1 (*6*) encodes a protein that shares amino acid sequence homology with GalT from *Escherichia coli* (PSI-BLAST E = 6e-21) (*7*). Because of its homology with GalT, the At5g18200.1 enzyme is annotated as a GalT-like protein. In particular, the $His^{184}Ser^{185}His^{186}Ser^{187}Gln^{188}$ motif in the At5g18200.1 protein is similar to the active site $His^{164}Pro^{165}His^{166}Gly^{167}Gln^{168}$ motif of GalT. The reaction

[†] Supported by NIH Grant GM30480 (P.A.F.), NIH Protein Structure Initiative Grants GM074901 and GM64598 (John L. Markley, principal investigator), and NLM Training Grant LM007359 (J.G.M.). Use of the Advanced Photon Source and the Argonne National Laboratory Structural Biology Center and sector-32 beamlines was supported by the U.S. Department of Energy, Office of Energy Research, under Contract W-31-109-ENG-38. Use of BioCARS was supported by the National Institutes of Health, National Center for Research Resources, via Grant RR07707. We gratefully acknowledge the Michigan Economic Development Corp. and the Michigan Technology Tri-Corridor for the support of this research program (Grant 085P1000817).

[‡] X-ray coordinates for the *Arabidopsis* At5g18200.1 protein have been deposited in the Protein Data Bank as entries 1ZWJ and 1Z84.

* To whom correspondence should be addressed: Department of Biochemistry, University of Wisconsin, 433 Babcock Dr., Madison, WI 53706-1544. Telephone: (608) 263-6142. E-mail: Phillips@biochem.wisc.edu.

[§] Department of Biochemistry.

[||] Center for Eukaryotic Structural Genomics.

[1] Abbreviations: ADP-glucose, adenosine 5′-diphosphate-α-D-glucose; UDP-glucose, uridine 5′-diphosphate-α-D-glucose; UDP-galactose, uridine 5′-diphosphate-α-D-galactose; NAD^+, nicotinamide adenine dinucleotide; $NADP^+$, nicotinamide adenine dinucleotide phosphate; NADH, reduced NAD^+; NADPH, reduced $NADP^+$; glucose-1-P, α-D-glucose 1-phosphate; galactose-1-P, α-D-galactose 1-phosphate; mannose-1-P, α-D-mannose 1-phosphate; GDP-mannose, guanosine 5-diphosphate-α-D-mannose; HEPES, *N*-(2-hydroxyethyl)piperazine-*N*′-4-butanesulfonic acid; EDTA, ethylenediaminetetraacetic acid; GalT, galactose-1-phosphate uridylyltransferase; HIT, histidine triad; P_i, inorganic phosphate; PEG, polyethylene glycol; SAD, single-wavelength anomalous dispersion; MES, 2-(*N*-morpholino)ethanesulfonic acid.

10.1021/bi052232m CCC: $33.50
Published on Web 02/17/2006

catalyzed by GalT proceeds by a double-displacement mechanism with a covalent uridylyl−enzyme intermediate, which involves the nucleophilic catalyst His^{166} (*8*−*10*).

In this paper, we describe the X-ray crystal structure of the At5g18200.1 protein and a covalent adenylyl−enzyme intermediate. We further describe the catalytic properties of the protein and show that it is not a GalT, but an adenylyltransferase that uses ADP-glucose as the donor substrate and catalyzes transfer of the adenylyl moiety to a broad range of phosphate acceptors. The best acceptor examined is phosphate itself, so the enzyme is an ADP-glucose phosphorylase. We demonstrate that the catalytic mechanism is analogous to that of GalT. We also show that the reaction preferably proceeds in the direction of the formation of ADP and glucose 1-phosphate from ADP-glucose and phosphate.

EXPERIMENTAL PROCEDURES

Materials. ADP-D-[U-^{14}C]glucose was purchased from Amersham Biosciences. Activated charcoal, $MgCl_2$, bicine, and EDTA were obtained from Aldrich Chemical Co. ADP, phosphoenolpyruvate, NADH, pyruvate kinase, HEPES, and lactic dehydrogenase were purchased from Sigma. Monobasic potassium phosphate, KCl, NaCl, NaOH, and HCl were obtained from Fisher Scientific. Microcon centrifugal filter devices were purchased from Amicon/Millipore.

Protein Expression and Purification. The At5g18200.1 gene was cloned into a pVP13 plasmid encoding a histidine$_6$−maltose binding protein tag according to the *E. coli*-based protocols described previously (*11*). Both unlabeled and selenomethionyl-labeled proteins were expressed according to the standard Center for Eukaryotic Structural Genomics protocol (*12*). Following sonication, the protein was purified via immobilized nickel affinity chromatography, and TEV protease was used to cleave the affinity/solubility tag (*13*). After tag capture and a final desalting step, the selenomethionyl-labeled protein was concentrated to 8.4 mg/mL and dialyzed against 50 mM NaCl and 5 mM HEPES (pH 7.0). The unlabeled protein sample was concentrated to 10.0 mg/mL and dialyzed against 50 mM NaCl and 5 mM Tris (pH 8.0).

Crystallization. Unlabeled and selenomethionyl At5g18200.1 protein crystals were grown by the hanging-drop vapor-diffusion method. The reservoir solution contained 20% (w/v) PEG 2000, 200 mM NaCl, and 100 mM MES-acetate (pH 5.5). Hanging drops consisted of 2 μL of protein solution mixed with 2 μL of reservoir solution. The crystals were grown at room temperature, and diffraction-quality specimens were obtained within 2−3 days. Crystals of the unliganded protein were then soaked in a series of reservoir solutions containing increasing amounts of ethylene glycol, up to a final concentration of 20% ethylene glycol, and were then flash-frozen in a stream of nitrogen. To prepare derivative crystals with the ligand, we first soaked them in a solution containing 20% (w/v) PEG 2000, 200 mM NaCl, 2 mM ADP-glucose, and 100 mM HEPES (pH 7.5) for a period of 2 h. Crystals were then cryoprotected and frozen as described above.

Data Collection and Reduction. Diffraction data for the native, unliganded structure were collected on beamline 14-ID-B BIOCARS at Argonne National Laboratory (Argonne, IL) at a wavelength of 0.9786 Å. Two data sets for the selenomethionyl-labeled, unliganded structure were collected on beamline 32-ID-B SBC at a wavelength of 0.9791 Å. The diffraction images were integrated and scaled using the HKL2000 package (*14*). Initial attempts to define the selenium substructure of the crystals failed. Therefore, a molecular replacement in Molrep (*6*, *16*) was attempted using the GALT dimer (PDB entry 1gup) as a search model. A very weak solution was obtained that provided the initial phase information necessary for the location of the strongest anomalous scatterers. The selenium substructure was completed with several cycles of SAD phasing and inspection of anomalous and gradient anomalous difference maps. The final set of anomalous scatterers was used for SAD phasing in CNS (*17*). Initial phase information to 3.5 Å was further improved and extended to the 2.4 Å resolution of the native data set by density modification and phase extension as implemented in CNS. The structure was built from the GALT dimer model and completed using alternate cycles of manual building in O (*18*) and Xfit (*19*) and crystallographic refinement in CNS. The native, liganded structure data were collected on beamline 19-BM SBC-CAT at Argonne National Laboratory at a wavelength of 0.97948 Å. HKL2000 was again used to integrate and scale the diffraction data, and initial phases were determined with MOLREP using the unliganded At5g18200.1 structure as the search model. Refinement was carried out using REFMAC (*16*, *20*), and the model was built with Xfit.

Assays. Adenylyltransferase activity was initially measured by the coupled assay employed for GalT, substituting ADP-glucose for UDP-glucose and using galactose-1-P, mannose-1-P, or P_i as the acceptor substrate (*8*). UV−visible spectrophotometry was performed on a Hewlett-Packard model 8452A diode array spectrophotometer.

The rate of glucose-1-P formation was measured by a coupled assay using $NADP^+$, phosphoglucomutase, and glucose-6-phosphate dehydrogenase. The assay was carried out in 1.0 mL containing 50 mM HEPES (pH 8.0), 1 mM $MgCl_2$, 0.1 mM EDTA, 0.5 mM $NADP^+$, 0.5 μM glucose 1,6-diphosphate, 0.1 unit/mL phosphoglucomutase, and 0.1 unit/mL glucose-6-phosphate dehydrogenase. The increase in A_{340} due to NADPH formation was used to calculate the glucose-1-P content of the aliquot, using 6.22 mM^{-1} cm^{-1} as the extinction coefficient.

The rate of ADP formation was measured enzymatically. The assay was carried out in 1.0 mL containing 50 mM HEPES (pH 7.0), 2 mM $MgCl_2$, 75 mM KCl, 0.2 mM NADH, 0.3 mM phosphoenolpyruvate, 1 unit/mL lactate dehydrogenase, and 1 unit/mL pyruvate kinase. The decrease in A_{340} due to consumption of NADH was used to calculate the amount of ADP in the aliquot, with 6.22 mM^{-1} cm^{-1} as the extinction coefficient.

Methods. The extinction coefficient for the At5g18200.1 protein at 280 nm was determined by the method of Gill and von Hippel (*21*). First, the value of ϵ_{280} for the denatured protein in 6 M guanidine-HCl (ϵ_{den}) was calculated from the number of tryptophan, tyrosine, and cysteine residues per molecule of the protein and their respective values of ϵ_{280}. Then absorbances at 280 nm of the native (Abs_{nat}) and denatured (Abs_{den}) proteins were measured at identical protein concentrations. The extinction coefficient for the native protein (ϵ_{nat}) was calculated using the equation $\epsilon_{nat} =$

Table 1: Summary of Crystal Parameters and Data Collection and Refinement Statistics (values in parentheses are for the highest-resolution shell)

	native	selenium 1	selenium 2	adenylylated native
space group	$P2_12_12_1$			
unit cell parameters (Å)	$a = 60.0$, $b = 95.5$, $c = 110.5$			$a = 62.0$, $b = 95.7$, $c = 110.9$
collection and phasing statistics				
wavelength (Å)	0.97858	0.97908	0.97908	0.97948
resolution range (Å)	27.59−2.30 (2.35−2.30)	46.99−3.20 (3.27−3.20)	48.57−3.20 (3.27−3.20)	34.49−1.83 (1.90−1.83)
no. of reflections (measured/unique)	177844/27575	153206/20251	150421/20137	399212/57501
completeness (%)	95.6 (80.4)	99.8 (100.0)	99.7 (100.0)	96.5 (71.4)
R_{merge}[a]	0.044 (0.406)	0.107 (0.284)	0.099 (0.305)	0.083 (0.386)
redundancy	6.4 (5.1)	7.6 (7.8)	7.5 (7.8)	6.9 (5.5)
mean $I/\sigma(I)$	24.03 (3.65)	16.95 (8.42)	17.20 (7.88)	15.24 (4.54)
refinement statistics				
resolution range (Å)	27.59−2.30			31.28−1.83
no. of reflections (total/test)	25918/2581			54539/2903
R_{cryst}[b]	0.215			0.186
R_{free}[c]	0.269			0.231
rmsd for bonds (Å)	1.3			1.558
rmsd for angles (deg)	0.006			0.017
average protein B factor (Å^2)	47.30			24.00
average solvent B factor (Å^2)	43.49			32.86
average substrate B factor (Å^2)				25.27

[a] $R_{merge} = \sum_h\sum_i|I_i(h) - \langle I(h)\rangle|/\sum_h\sum_i I_i(h)$, where $I_i(h)$ is the intensity of an individual measurement of the reflection and $\langle I(h)\rangle$ is the mean intensity of the reflection. [b] $R_{cryst} = \sum_h||F_{obs}| - |F_{calc}||/\sum_h|F_{obs}|$, where F_{obs} and F_{calc} are the observed and calculated structure factor amplitudes, respectively. [c] R_{free} was calculated as R_{cryst} using 5.0% of the randomly selected unique reflections that were omitted from structure refinement.

$(Abs_{nat}\epsilon_{den})/Abs_{den}$. The ϵ_{nat} value determined for the At5g18200.1 monomer was 32.0 ± 0.4 mM^{-1} cm^{-1}.

The equilibrium constant for the reaction of ADP-glucose with P_i to produce ADP and glucose-1-P was evaluated as follows. The reaction was allowed to proceed for 20 min to reach equilibrium followed by heating in boiling water for 5 min to inactivate the enzyme. The reaction mixtures (2.0 mL) initially contained 0.1 M HEPES (pH 7.0), 0.1 mM P_i, 0.05 mM ADP-glucose, and 25 μg/mL ADP-glucose phosphorylase. After centrifugation of the coagulated enzyme (10 min at 14 000 rpm), aliquots of the supernatant fluid were enzymatically assayed for glucose-1-P and ADP content. To study the effect of Mg^{2+}, the experiment was also performed in the presence of 1 mM $MgCl_2$. These experiments were carried out under variable concentrations of substrates and enzyme and also for longer reaction times. The results showed that equilibrium had been attained under all conditions that were employed.

Steady State Kinetics. A radiochemical method for assaying GalT (*8*) was adapted to measuring the initial rates of the reaction of ADP-glucose with P_i to form ADP and glucose-1-P. Each reaction mixture (1.5 mL) contained 0.1 M sodium bicinate (pH 8.5), 5−60 μM inorganic phosphate, 0.2−7.0 μM ADP-[^{14}C]glucose (3.7×10^6 to 2.6×10^7 cpm/μmol), and 6.7 nM At5g18200.1 enzyme. The reactions were started by addition of the enzyme. At predetermined times, aliquots of the reaction mixture were added to 20 mg of activated charcoal and mixed thoroughly to stop the reaction. The mixtures were centrifuged and the supernatant fluids filtered, using Microcon YM-50 centrifugal filter devices. Aliquots of filtrates were assayed radiochemically for ^{14}C using liquid scintillation counting on a Beckman LS 6500 spectrometer. Progress curves were linear and gave the initial rates.

The initial rates for the exchange of [^{14}C]glucose between ADP-glucose and glucose-1-P were measured by the charcoal-quench method described above for the overall reaction. In this case, the reaction mixtures (1.5 mL) contained 0.1 M sodium bicinate (pH 8.5), 10−400 μM glucose-1-P, 0.25−1.0 μM ADP-[^{14}C]glucose (2.8×10^7 cpm/μmol), and 8.0 nM At5g18200.1 enzyme. The linear progress curves yielded initial rates.

Data Analysis. The initial rate data were computer fitted to eq 1 for the ping-pong mechanism using the PNGPNG program of Cleland (*22*):

$$v = (V_m[A][B])/(K_a[B] + K_b[B] + [A][B]) \quad (1)$$

where A and B refer to ADP-glucose and P_i, respectively. Values of v are the experimental initial rates. k_{cat} values were obtained through the division of V_m values by the enzyme concentration.

RESULTS

Structure Determination. The structure of the At5g18200.1 protein has been determined to a resolution of 2.30 Å. The relevant statistics are given in Table 1. The protein forms a dimer with each chain comprising 351 amino acids. The asymmetric unit contains the biological homodimer, labeled as chains A and B. Several surface loops were not modeled due to insufficient electron density. These include amino acids 1−22, 40−47, 52−61, and 106−115 of chain A as well as residues 1−20, 40−45, 51−61, 68−71, 106−115, and 351 of chain B. A Ramachandran plot indicates 557 of the 600 modeled amino acids are in the most favored $\phi-\psi$ regions with the remainder falling in the generously allowed regions. The asymmetric unit also contains 225 ordered water molecules. Each monomer in the asymmetric unit coordinates two zinc atoms via two cysteine and two histidine side chains.

Protein Fold. The overall fold of the monomer is shown in Figure 1 and consists of an antiparallel open-faced β-pleated sheet formed by β-strands C, D, F, H, G, L, M,

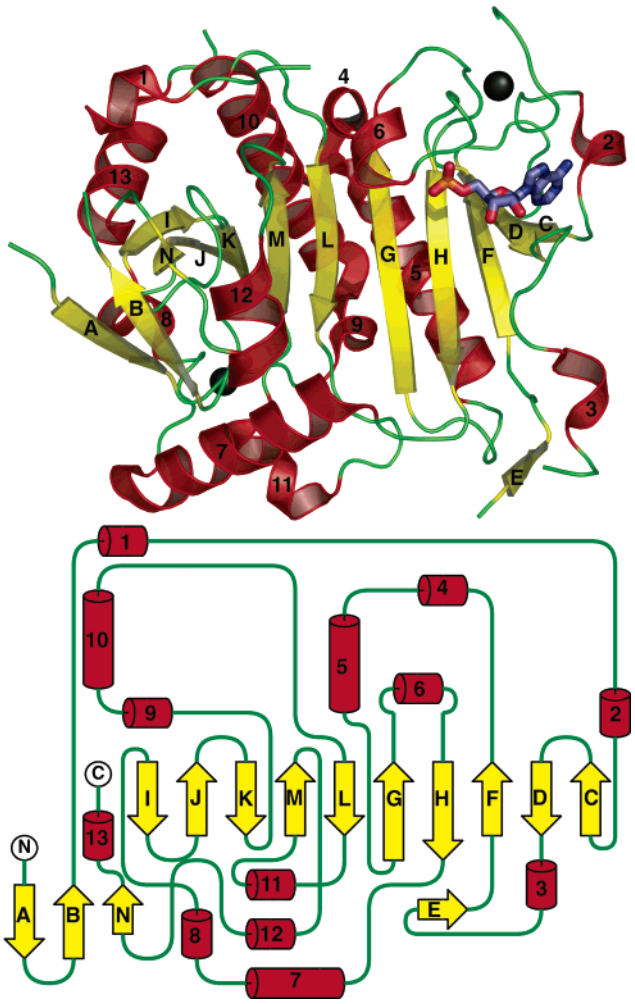

FIGURE 1: Ribbon and topology diagrams of the At5g18200.1 protein. Depicted is chain A of the adenylylated monomer. Zinc atoms are shown as gray spheres, and the AMP group is shown as a stick model. Both ribbon and topology diagrams are labeled in an identical manner using A−N for the β-strands and 1−13 to distinguish the helices. This figure was prepared using Pymol (*35*) and Topdraw (*36*).

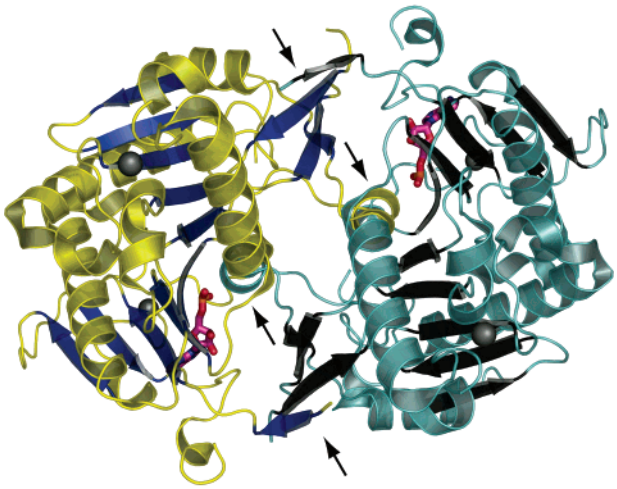

FIGURE 2: Dimer interface of the At5g18200.1 protein. Depicted is the At5g18200.1 dimer along the 2-fold symmetry axis with chain A (yellow and blue) and chain B (cyan and black) in a ribbon representation. Zinc ions are shown as gray spheres, and the adenylyl intermediate is shown as a stick model. The active site of each subunit is located along the exterior of the GalT-like half-barrel and positioned near the dimer interface. Arrows specify regions of contact between the two monomers, namely, the interchain β-sheets formed by strands A, B, N, and E and α-helix 12. This figure was generated with Pymol (*35*).

Table 2: Nucleotidyl Donor Activities of the At5g18200.1 Enzyme

donor substrate	acceptor substrate	activity [μmol min^{-1} (mg of protein)$^{-1}$][a]
UDP-glucose[b]	galactose-1-P[c]	0.0097
ADP-glucose[d]	galactose-1-P[e]	0.086
ADP-glucose[d]	mannose-1-P[c]	0.24
ADP-glucose[d]	P_i[f]	7.1
ADP-glucose[d]	$MgPP_i$[g]	none detected

[a] Rates of glucose-1-P production measured at pH 8.5 in sodium bicinate buffer at 27 °C as described in Experimental Procedures. [b] At 50 μM. [c] At 200 μM. [d] At 20 μM. [e] At 250 μM. [f] At 31 μM. [g] At 100 μM.

K, J, and I that surround two antiparallel amphipathic helices (5 and 10) that overlap near their N-termini forming an angle of roughly 50°. Short helices (4 and 9) are positioned roughly 90° from the primary axes of helices 5 and 11 such that their amino termini point directly toward the β-sheet. The remaining β-strands form a mixed intersubunit β-sheet which consists of strands A, B, and N of one monomer and strand E from the other. Strand B also makes contacts with a turn from the opposing chain. In addition, the protrusion containing helix 12 makes extensive contacts with helix 6, the loop running from the carboxy terminus of strand H to the amino terminus of helix 7, and β-strands M, L, and G of the other monomer (see Figure 2). The average buried solvent accessible surface area of the interface is 1955 Å^2.

Catalyzed Reaction. Since the At5g18200.1 protein is annotated as a GalT-like uridylyltransferase, the enzyme was tested for GalT activity. GalT catalyzes the conversion of UDP-glucose and galactose-1-P into glucose-1-P and UDP-galactose. The production of glucose-1-P forms the basis for the standard assay (*8*). The coupled assay includes phosphoglucomutase, glucose-6-P dehydrogenase, and $NADP^+$ and measures the level of glucose-1-P formation through formation of NADPH. Surprisingly, the At5g18200.1 protein displays less than 5×10^{-5} of the activity of *E. coli* GalT. Therefore, we performed detailed substrate specificity studies. These studies reveal adenylyltransferase activity with ADP-glucose as the donor and galactose-1-P as the acceptor. Typical results shown in Table 2 indicate that the At5g18200.1 enzyme is almost 10 times more active in the GalT assay with ADP-glucose as the donor substrate, and it is another 2.8 times more active with mannose-1-P as the acceptor substrate. The preferential utilization of ADP-glucose and mannose-1-P rather than UDP-glucose and glucose-1-P clearly shows that the At5g18200.1 enzyme does not possess GalT activity. ADP-glucose and inorganic phosphate are the best donor and acceptor substrates, respectively, so far tested. The entries in Table 2 show the activity with ADP-glucose and P_i to be more than 700 times that with UDP-glucose and galactose-1-P. The enzyme does not display ADP-glucose pyrophosphorylase activity, as shown by the fact that $MgPP_i$ does not serve as an acceptor.

In preliminary experiments to narrow the focus on substrate preference, apparent values of V_{max} and K_m confirm and quantify the preferences implied by the survey data in Table 2. Assaying for glucose-1-P production from ADP-glucose, at 1 mM galactose-1-P, we find a value of K_m^{app}

for ADP-glucose of 7 μM, and at 5 μM ADP-glucose, the value of K_m^{app} for galactose-1-P is 2 mM. In contrast, the value of K_m^{app} for P_i is 18 μM at 20 μM ADP-glucose. When rates are compared, at 5 μM ADP-glucose, the value of the apparent second-order rate constant $[(k_{cat}/K_m)^{app}]$ for the reaction of galactose-1-P is 3×10^2 M^{-1} s^{-1}, and that for the reaction of P_i at 20 μM ADP-glucose is 4×10^5 M^{-1} s^{-1}. These constants cannot be compared directly because of the 4-fold difference in concentrations of ADP-glucose. However, even if the value for P_i were 4-fold lower (this would be the maximum normalization), the ratio of apparent second-order rate constants would be more than 300 in favor of the reaction of P_i. It must be concluded that the At5g18200.1 enzyme is not a GalT, nor an ADP-glucose pyrophosphorylase, but it is an adenylyltransferase that displays selectivity for ADP-glucose and P_i as donor and acceptor substrates, respectively.

Kinetic Mechanism. The reactions catalyzed by the At5g18200.1 enzyme and GalT are chemically similar, in that both catalyze nucleotidyl transfer with nucleotide sugars as donor substrates and phosphates as acceptors. Therefore, given the sequence and structure homology, the chemical and kinetic mechanisms might be analogous. If so, the adenylyltransferase should function by a double-displacement chemical mechanism and ping-pong kinetics through a covalent nucleotidyl−enzyme intermediate, as does GalT. Alternatively, the reaction might proceed by a sequential kinetic mechanism characteristic of UDP-glucose pyrophosphorylase and ADP-glucose pyrophosphorylase, with no covalent intermediate. Steady state kinetic analysis distinguishes these mechanisms.

Equations 2 and 3 describe the hypothetical double-displacement mechanism with ping-pong kinetics for the action of the At5g18200.1 enzyme, where His^{186} is the central histidine in the putative catalytic $His^{184}Ser^{185}His^{186}Ser^{187}$-$Gln^{188}$ motif.

$$\text{E-His}^{186} + \text{ADP-glucose} \rightleftharpoons \text{E-His}^{186}\text{-AMP} + \text{glucose-1-P} \quad (2)$$

$$\text{E-His}^{186}\text{-AMP} + P_i \rightleftharpoons \text{E-His}^{186} + \text{ADP} \quad (3)$$

According to this mechanism, the enzyme must catalyze the exchange of ^{14}C between ADP-[^{14}C]glucose and glucose-1-P in the absence of P_i with ping-pong kinetics and at a rate that is compatible with the rate of the overall reaction. The At5g18200.1 enzyme satisfies both criteria, as shown in Figure 3, where the reciprocals of the initial rates of exchange are plotted against the reciprocal of the concentration of glucose-1-P at three fixed concentrations of ADP-[^{14}C]glucose. The observation of exchange supports eq 2 as a step in the kinetic mechanism, and the parallel line pattern supports the ping-pong kinetic mechanism with a covalent AMP-enzyme as an intermediate. The kinetic parameters for the exchange reaction, obtained by fitting the data presented in Figure 3 to eq 1 for the ping-pong kinetic mechanism, are given in Table 3.

If the kinetic and chemical mechanism of eqs 2 and 3 is correct, the steady state kinetics of the overall reaction must also conform to eq 1. As shown in Figure 4, the double-reciprocal plot of steady state kinetic data is a set of parallel lines corresponding to eq 1. When fitted to the data in Figure 4, the kinetic parameters in Table 3 are obtained. Comparison with the parameters for the ADP-[^{14}C]glucose−glucose-1-P exchange shows that the exchange reaction is faster, so the exchange rate is kinetically compatible with the rate and mechanism of the overall reaction. The kinetics of the exchange and overall reactions strongly support the ping-

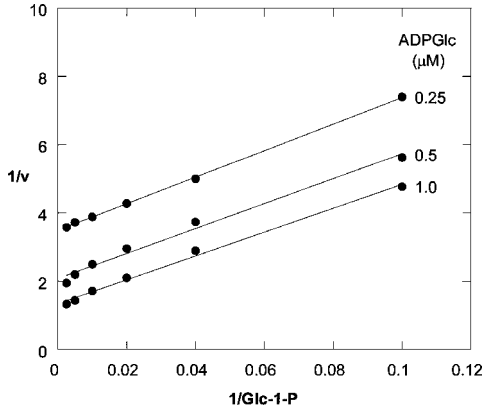

FIGURE 3: Initial rates for exchange of ^{14}C from ADP-[^{14}C]glucose into glucose-1-P. The initial rates were measured as described in Experimental Procedures and plotted in double-reciprocal form. The ADP-[^{14}C]glucose (2.8×10^7 cpm/μmol) concentrations were 0.25−1.0 μM, and glucose-1-P concentrations were 10−400 μM. The velocity units are micromolar per minute with 8.1×10^{-3} μM At5g18200.1 enzyme. The parameters resulting from fitting eq 1 to the data are listed in Table 3.

Table 3: Kinetic Parameters for Reactions of the At5g18200.1 Enzyme

reaction	k_{cat} (s^{-1})	$K_m^{ADP-glucose}$ (μM)	K_m^{P} (μM)	$K_m^{glucose-1-P}$ (μM)
overall[a]	2.7 ± 0.4	6.9 ± 1.2	90 ± 19	−
exchange[b]	4.1 ± 0.3	1.4 ± 0.2	−	83 ± 8

[a] Reaction of ADP-glucose with P_i to form ADP and glucose-1-P at pH 8.5 and 25 °C. [b] Exchange of ^{14}C from ADP-[^{14}C]glucose to glucose-1-P at pH 8.5 and 25 °C.

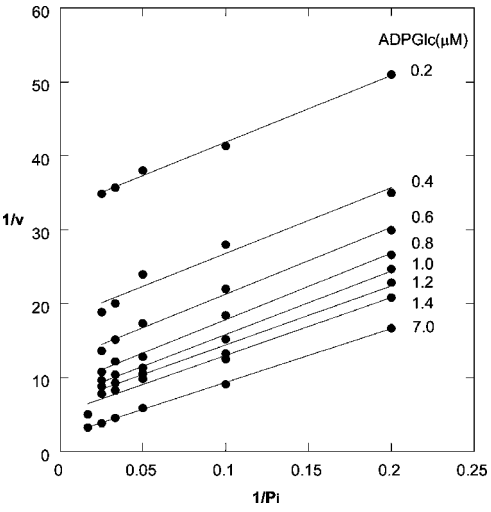

FIGURE 4: Initial rates of glucose-1-P formation in the action of the At5g18200.1 enzyme. Initial rates of glucose-1-P formation at varying ADP-[^{14}C]glucose concentrations and several fixed P_i concentrations were measured as described in Experimental Procedures and plotted in double-reciprocal form. The ADP-[^{14}C]-glucose concentrations were 0.2−7.0 μM, and P_i concentrations were 5−60 μM. The velocity units are micromolar per minute at 6.7×10^{-3} μM At5g18200.1 enzyme. The parameters resulting from fitting eq 1 to the data are listed in Table 3.

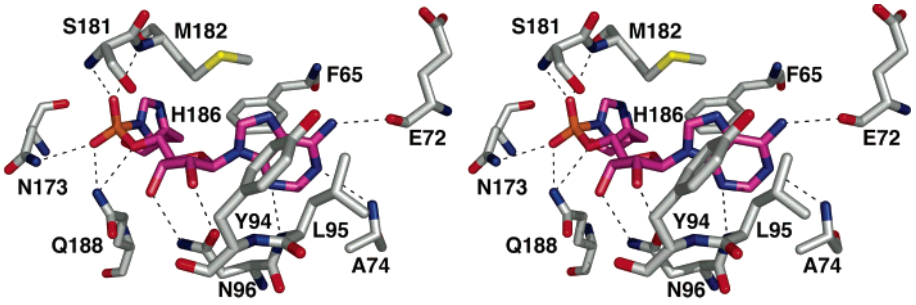

FIGURE 5: Active site of the At5g18200.1 enzyme. Illustrated are the interactions between the enzyme active site and the AMP−histidine intermediate (magenta) formed upon addition of ADP-glucose. This figure was generated with Pymol (*35*).

pong kinetic mechanism and the chemistry of eqs 2 and 3, and they rule out all sequential kinetic mechanisms.

According to the kinetic mechanism, the reaction of the At5g18200.1 enzyme with ADP-glucose must produce the covalent adenylyl−enzyme intermediate. In this study, this intermediate is isolated and characterized by X-ray crystallography in work that is described in a later section.

Equilibrium Constant (K_{eq}). The reaction of ADP-glucose with P_i to form ADP and glucose-1-P should be energetically reasonably balanced. We measured the value of K_{eq} at pH 7.0 in the absence of Mg^{2+} and found it to be 5.0 ± 0.3. While the reaction to form glucose-1-P is fairly well favored, Mg^{2+} should draw it much further to completion because of the formation of MgADP and the relatively weak binding of Mg^{2+} to ADP-glucose. Accordingly, the value of K_{eq} in the presence of 1 mM $MgCl_2$ is 40 ± 1. Thus, in the presence of 1 mM Mg^{2+}, the reaction is strongly favored in the forward direction, with a $\Delta G°'$ value of −2.2 kcal/mol.

Crystallographic Isolation of the AMP−Enzyme Intermediate. The covalently modified enzyme structure was determined to a resolution of 1.83 Å (Table 1). The electron density for AMP was clearly evident in the electron density map. The α-phosphorus of AMP was refined to a position 1.8 Å from NE2 of His^{186} in chain A and 1.7 Å in chain B. The coordination of AMP is identical in both chains A and B. A number of hydrogen bonds are observed coordinating the AMP molecule (see Figure 5). The side chain amines of Gln^{188} and Asn^{173} both coordinate with one of the oxygens of the α-phosphate of AMP. In addition, a solvent molecule is within hydrogen bonding distance of both the oxygen and the backbone amine of Asn^{173} (not shown). Gln^{188} appears to make a second contact with the bridging oxygen of AMP as well. The other phosphate oxygen is within hydrogen bonding distance of the backbone amines of Ser^{181} and Met^{182}. The side chain of Asn^{96} is within hydrogen bonding distance of O2′ and O3′ of the ribose sugar. The adenine group is coordinated to the backbone amines of Ala^{74} and Leu^{95} and the backbone carbonyl group of Glu^{72}. Additional stabilization is provided by "T stacking interactions" through the side chains of Phe^{65} and Tyr^{94}.

DISCUSSION

Protein Fold. The overall fold of the At5g18200.1 protein is quite similar to that of the *E. coli* GalT (DALI score = 31.8). The largest discernible difference between the two monomers is between residues 70 and 90 of the *Arabidopsis* protein and the analogous region in GalT. This region corresponds to strand C in the At5g18200.1 enzyme but in GalT forms a small two-stranded β-sheet. A further difference is that the buried surface area between the At5g18200.1 monomers is only slightly more than half the value reported for the GalT dimer. The difference appears to be due mainly to the missing loops of the At5g18200.1 protein, which in GalT are involved in the dimer interface but for which there was insufficient electron density to build into the At5g18200.1 protein model.

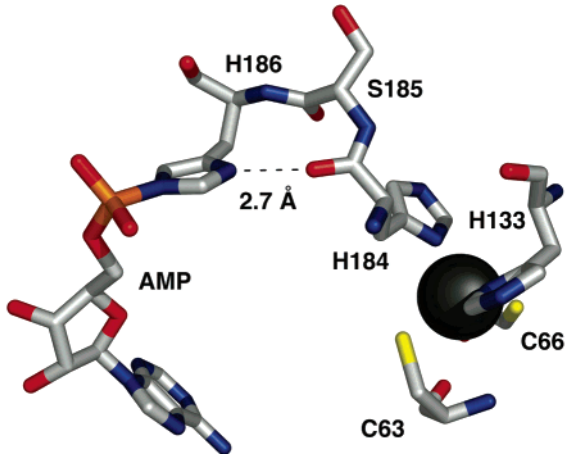

FIGURE 6: Role of zinc in catalysis. The zinc ion bound by the side chain of His^{184} may be necessary for positioning the main chain carbonyl oxygen of His^{184} 2.7 Å from ND1 of His^{186} in chain A (2.8 Å in chain B). This interaction may help stabilize the His−AMP intermediate. Zinc is depicted as a gray sphere. This figure was generated with Pymol (*35*).

Zinc Binding Sites. In addition, there is a difference in metal binding between the two enzymes. The *E. coli* GalT monomer contains both a zinc and an iron atom (*23*); the identities of these metals have been confirmed by inductively coupled plasma emission spectroscopy (*24*). It has been further shown that enzyme activity is dependent on the occupation of the zinc binding site; however, a variety of metals appear to support catalysis (*24*, *25*). The two metal ions in each At5g18200.1 protein subunit were assumed to be zinc on the basis of their coordination and anomalous signal.

One of the zinc sites is identical to the zinc site found in GalT, directly adjacent to the active site. Figure 6 depicts the coordination of the zinc ion in the At5g18200.1 enzyme and illustrates its possible role in catalysis. As originally seen and described in the *E. coli* GalT structure (*26*), the zinc appears to be positioning the carbonyl of His^{184} within hydrogen bonding distance of ND1 of His^{186}. This may be critical for stabilizing the nucleotidylated intermediate and allowing the reaction to proceed.

The second zinc atom is located in a position different from that of the iron atom from GalT, although they share

```
Arabidopsis thaliana          65 FCIGREQECAPELFRVP-----DHDPNWKLRVIENL  95
Lycopersicon esculentum          FCAGHEHECAPEIFRVPA----DSTNDWKIRVIQNL
Solanum tuberosum                FCAGHEHECAPEIFRVPA----DSTNDWKIRVIQNL
Vitis vinifera                   FCSGHEHECAPEIFRFPP----DSTVDWKIRVIQNL
Oryza sativa                     FCQGRESECAPEIFRVPAP---PDASPWRIRVIENL
Triticum aestivum                FCLGRESECAPEIFRVPPP---DASPPWRIRVIENL
Thermatoga maritima           42 FDYGNEHTTPPEIFAFRPADTEPNTPGWWVRVVPNK  77
Pelobacter propionicus        41 FCYGNEDKTPPEIFAIRPSG-MPNAANWRVRVIPNK  75
Thiobacillus denitrificans    54 FCRGNEDKTPPAILAWPES------ADWQIRMVENL  83
Escherichia coli              54 LCAGNVRVTGDKNPDYT-----------GTYVFTND  78
Homo sapiens                  74 LCPGAIRANGEVNPQYD-----------STFLFDND  98

Arabidopsis thaliana         167 YIQVFKNQGASAGASMSHSHSQMMALPVVPPTVSSR 202
Lycopersicon esculentum          YVQVFKNHGASAGASMSHSHSQMIALPIVPPTVSAR
Solanum tuberosum                YVQVFKNHGASAGASMSHSHSQMIALPIVPPTVSAR
Vitis vinifera                   YIQVFKNHGASAGASMSHSHSQIMALPIVPPTVSSR
Oryza sativa                     TGMVFKNHGASAGASMAHSHSQMLGTPFVPPSVTTR
Triticum aestivum                YVQVFKNQGASAGASMAHSHSQMLGTPFVPPSVTSR
Thermotoga maritima          147 YILIFKNHGRDAGASLSHPHSQIIALPIMPKRVQEE 182
Pelobacter propionicus       145 YMVIFKNHGLRAGATLHHSHSQLIAVPLLPPVAATE 180
Thiobacillus denitrificans   155 YVLVFKNFGPAAGASIPHTHSQVIAMPVVPENVEAE 190
Escherichia coli             147 WVQVFENKGAAMGCSNPHPHGQIWANSFLPNEAERE 182
Homo Sapiens                 147 WVQIFENKGAMMGCSNPHPHCQVWASSFLPDIAQRE 182
```

FIGURE 7: Portion of the sequence alignment between uridylyltransferases and putative adenylyltransferases. The At5g18200.1 enzyme and all putative adenylyltransferases from plant species are labeled in green. Putative adenylyltransferases from bacteria are labeled in red. Sequence labels for confirmed uridylyltransferases are colored blue. Residues that appear to distinguish adenylyltransferases from uridylyltransferases are colored orange. The top block of sequences corresponds to the adenine/uridine binding region. The bottom block corresponds to the region that contains the HXHXQ active site motif. The start codon for some of the sequences was unclear, and subsequently, no residue numbering was included. The alignment was created with ClustalW (*37*). The sequence codes for the sequences included in the alignment are as follows: NP_197321 (GenBank), TC156309 (TIGR), TC113581 (TIGR), TC40775 (TIGR), 9635.m00702 (Plastid Proteome Database), TC237707 (TIGR), NP_228704 (GenBank), EA03679 (GenBank), AAF64398 (GenBank), P09148 (UniProt), and P07902 (UniProt).

one liganding side chain. The side chain of His^{310} in the At5g18200.1 enzyme is oriented differently from its conserved sequence counterpart in GalT, subsequently shifting the metal binding site 12.5 Å from where it is located in GalT toward the surface of the protein. It was proposed that the iron atom in GalT plays a role in stabilizing the domain-swapped dimer interface (*23*), but in the At5g18200.1 enzyme, this appears less likely.

Enzyme Activity. The ADP-glucose phosphorylase activity of the At5g18200.1 enzyme is the same as that described 40 years ago for an ADP-glucose:orthophosphate adenylyltransferase in extracts of wheat germ (*27*). The wheat germ enzyme was partially purified and shown to accept ADP-1′α-D-glucose, 2′-deoxy-ADP-1′α-D-glucose, and ADP-1′β-D-glucose as adenylyl group donors; however, it was not purified to homogeneity. Both the At5g18200.1 enzyme and the wheat germ adenylyltransferase display the activity corresponding to the systematically named ADP:α-D-aldose-1-phosphate adenylyltransferase (EC 2.7.7.36). No information about the kinetic or chemical mechanism is available for the wheat germ enzyme.

Production of glucose-1-P without pyrophosphate (which is required by the enzyme ADP-glucose pyrophosphorylase) has been reported for several plant extracts, including barley and *Arabidopsis* (*28*). In that study, the authors isolated and purified a 35 kDa enzyme from barley leaves that they identified as an ADP-glucose pyrophosphatase, catalyzing the hydrolysis of ADP-glucose into glucose-1-P and AMP. Addition of phosphate was shown to competitively inhibit the enzyme. No sequence was given for the barley enzyme, but it seems unlikely that this protein is identical to the At5g18200.1 enzyme despite the possibility that they serve a similar role in regulating starch production.

A partially purified adenylyltransferase from *Euglena gracilis* catalyzes the reaction of ADP-5′-ribose with phosphate to form ADP and ribose 1,5-bisphosphate (*29*). This enzyme catalyzes the ADP−P_i exchange in the absence of ribose 1,5-bisphosphate, apparently by the mechanism of eq 3. The *Euglena* adenylyltransferase does not accept ADP-glucose as a substrate, so it cannot be the same as the enzyme described here, although the reaction mechanisms may be similar. However, the At5g18200.1 enzyme efficiently catalyzes the phosphorolysis of ADP-5′-ribose (data not shown).

The activity of the At5g18200.1 enzyme is analogous to previously reported nucleotide sugar phosphorolysis activities of enzymes displaying substrate preferences for GDP-mannose and UDP-glucose (*30*). These enzymes also catalyze exchange reactions such as UDP−P_i exchange which is analogous to the ADP-glucose−glucose-1-P exchange described here for the At5g18200.1 enzyme.

Sequence Analysis. A series of BLAST searches using the entire At5g18200.1 enzyme sequence, as well as a portion of the sequence corresponding to the enzyme's adenine binding region, resulted in the identification of a number of plant and bacterial enzymes which may be functionally similar to At5g18200.1. A partial sequence alignment containing a representative sample of these enzymes (Figure 7) reveals a number of residues that may prove to be useful in distinguishing between uridylyltransferases and adenylyltransferases. All of these enzymes are annotated as putative galactose-1-P uridylyltransferases with the exception of those from *E. coli* and *Homo sapiens*, which are confirmed galactose-1-P uridylyltransferases, and the enzyme from *Thiobacillus denitrificans* which is annotated as an adenylylsulfate:phosphate transferase.

The At5g18200.1 enzyme residues that appear to be unique for adenylyltransferases include Phe^{65}, which is involved in stabilizing the adenine ring through stacking interactions. Residues homologous to Glu^{70}, Trp^{87}, and Arg^{90} are also strongly conserved. These residues correspond to a region of the At5g18200.1 enzyme that is structurally distinct from GalT of *E. coli*. Specifically, an extended loop between helix 2 and strand C makes additional contacts with the adenine group (Figure 1). The side chains of Glu^{70}, Trp^{87}, and Arg^{90} are involved in hydrogen bonding interactions that may help stabilize this extended loop. Asp^{98} (*E. coli*) is a unique, strongly conserved residue in GalT enzymes. This residue coordinates the uridine group in the *E. coli* structure (*26*) but is converted to either a leucine or lysine in the putative adenylyltransferase sequences.

We do not have enough data to distinguish between enzymes with adenylylsulfate:phosphate transferase activity and enzymes with ADP-glucose phosphorylase activity through sequence alignments. The glucose binding region would be the most likely place to distinguish between these activities as the adenylylsulfate:phosphate transferase would have no need to bind glucose. The sequences of the glucose binding regions of potential adenylyltransferases and uridylyltransferases are surprisingly different; however, many of the interactions with glucose in the *E. coli* GalT structure involved backbone atoms (*31*). Structural alignment of GalT and the At5g18200.1 protein reveals that the positions of the relevant backbone atoms are in identical positions despite the low level of sequence conservation. Of the five residues in GalT with side chains coordinated to glucose, four are conserved in every sequence, including that of adenylylsulfate:phosphate transferase. As a result, it is difficult to distinguish between adenylylsulfate:phosphate transferases and ADP-glucose phosphorylases. In addition, all of the putative adenylyltransferases have two cysteine and two histidine residues corresponding to those involved in coordinating the second zinc atom in the At5g18200.1 enzyme, and all are missing one or more residues needed for coordinating iron as in the *E. coli* GalT structure (*23*).

Possible Role in Starch Synthesis. The biological function of the At5g18200.1 protein cannot be assigned solely on the basis of in vitro biochemical properties. The catalyzed reaction represents a means of degrading ADP-glucose in such a way as to conserve the free energy of the phosphoanhydride and aldose 1-phosphate linkages. On this basis, we hypothesize that this enzyme participates in ADP-glucose homeostasis. ADP-glucose is known to play a prominent role in starch metabolism in plants (*32*). ADP-glucose is synthesized by the enzyme ADP-glucose pyrophosphorylase (APGase) and is then polymerized via the soluble and granule-bound starch synthases (*33*). While most evidence has suggested that these reactions take place entirely in the plastids of noncereal plants, such as *Arabidopsis*, recent studies have suggested that ADP-glucose may also be synthesized in the cytosol and transported into the plastid (*34*, *35*).

The At5g18200.1 enzyme is not currently implicated in this regulation. Also, the conditions under which and the cellular compartments of *Arabidopsis* in which the At5g18200.1 enzyme is normally produced are not known. Moreover, although the enzyme is quite active with ADP-glucose and P_i ($k_{cat}/K_m = 0.4 \times 10^6\ s^{-1}\ M^{-1}$ for the reaction of ADP-glucose at saturating P_i concentrations), there could be even better substrates. We can assert that whenever this enzyme is present with ADP-glucose, P_i, and Mg^{2+} the ADP-glucose will be converted to ADP and glucose-1-P. Biological experiments, including gene deletions, will be required to deduce the biological function of the *Arabidopsis* At5g18200.1 enzyme.

In conclusion, we have determined the structure of the At5g18200.1 protein and established its structural homology to *E. coli* GalT. We have shown that the enzyme does not possess GalT activity but instead displays adenylyltranferase activity. We have further shown that, of the substrates tested, the enzyme displays the greatest activity when ADP-glucose and P_i are used as the donor and acceptor, respectively, making the enzyme an ADP-glucose phosphorylase, or ADPGPase. We have determined kinetic and equilibrium constants for this reaction and shown that the reaction proceeds through a bi-bi double-displacement mechanism. We have also isolated and observed the enzyme−AMP intermediate suggested by this mechanism through X-ray crystallography.

ACKNOWLEDGMENT

We thank 19-BM SBC beamline scientists Randy Alkire, Ph.D., and Stephan L. Ginell, Ph.D., for help we have received during data collection. We specially thank members of the CESG team: Craig S. Newman, Zhaohui Sun, Russell L. Wrobel, Eric Steffan, Zachary Eggers, Megan Riters, Ronnie O. Frederick, John Kunert, Hassan Sreenath, Brendan T. Burns, Kory D. Seder, Holalkere V. Geetha, Frank C. Vojtik, Won Bae Jeon, Jason M. Ellefson, Andrew C. Olson, Janet E. McCombs, David J. Aceti, Janelle Warick, Bryan Ramirez, Gary Wesenberg, Zsolt Zolnai, Peter T. Lee, Mike Runnels, John Cao, Jianhua Zhang, John Primm, Donna Troestler, Michael R. Sussman, Brian G. Fox, and John L. Markley.

REFERENCES

1. Gough, J., Karplus, K., Hughey, R., and Chothia, C. (2001) Assignment of homology to genome sequences using a library of hidden Markov models that represent all proteins of known structure, *J. Mol. Biol. 313*, 903−919.
2. Brenner, C., Garrison, P., Gilmour, J., Peisach, D., Ringe, D., Petsko, G. A., and Lowenstein, J. M. (1997) Crystal structures of HINT demonstrate that histidine triad proteins are GalT-related nucleotide-binding proteins, *Nat. Struct. Biol. 4*, 231−238.
3. Brenner, C. (2002) Hint, Fhit, and GalT: Function, structure, evolution, and mechanism of three branches of the histidine triad superfamily of nucleotide hydrolases and transferases, *Biochemistry 41*, 9003−9014.
4. Bruser, T., Selmer, T., and Dahl, C. (2000) "ADP sulfurylase" from *Thiobacillus denitrificans* is an adenylylsulfate:phosphate adenylyltransferase and belongs to a new family of nucleotidyltransferases, *J. Biol. Chem. 275*, 1691−1698.
5. Booth, J. W., and Guidotti, G. (1995) An alleged yeast polyphosphate kinase is actually diadenosine-5′,5‴-P1,P4-tetraphosphate α,β-phosphorylase, *J. Biol. Chem. 270*, 19377−19382.
6. Dennis, C., and Surridge, C. (2000) *Arabidopsis thaliana* genome. Introduction, *Nature 408*, 791.
7. Altschul, S. F., Madden, T. L., Schaffer, A. A., Zhang, J., Zhang, Z., Miller, W., and Lipman, D. J. (1997) Gapped BLAST and PSI-BLAST: A new generation of protein database search programs, *Nucleic Acids Res. 25*, 3389−3402.
8. Wong, L. J., and Frey, P. A. (1974) Galactose-1-phosphate uridylyltransferase: Rate studies confirming a uridylyl-enzyme intermediate on the catalytic pathway, *Biochemistry 13*, 3889−3894.

9. Wong, L. J., and Frey, P. A. (1974) Galactose 1-phosphate uridylyltransferase. Isolation of a uridylyl-enzyme intermediate, *J. Biol. Chem. 249*, 2322−2324.
10. Wong, L. J., Sheu, K. F., Lee, S. L., and Frey, P. A. (1977) Galactose-1-phosphate uridylyltransferase: Isolation and properties of a uridylyl-enzyme intermediate, *Biochemistry 16*, 1010−1016.
11. Thao, S., Zhao, Q., Kimball, T., Steffen, E., Blommel, P. G., Riters, M., Newman, C. S., Fox, B. G., and Wrobel, R. L. (2004) Results from high-throughput DNA cloning of *Arabidopsis thaliana* target genes using site-specific recombination, *J. Struct. Funct. Genomics 5*, 267−276.
12. Sreenath, H. K., Bingman, C. A., Buchan, B. W., Seder, K. D., Burns, B. T., Geetha, H. V., Jeon, W. B., Vojtik, F. C., Aceti, D. J., Frederick, R. O., Phillips, G. N., Jr., and Fox, B. G. (2005) Protocols for production of selenomethionine-labeled proteins in 2-L-polyethylene terephthalate bottles using auto-induction medium, *Protein Expression Purif. 40*, 256−267.
13. Jeon, W. B., Aceti, D. J., Bingman, C. A., Vojtik, F. C., Olson, A. C., Ellefson, J. M., McCombs, J. E., Sreenath, H. K., Blommel, P. G., Seder, K. D., Buchan, B. W., Burns, B. T., Geetha, H. V., Harms, A., Sabat, G., Sussman, M. R., Fox, B. G., and Phillips, G. N., Jr. (2005) High-throughput purification and quality assurance of *Arabidopsis thaliana* proteins for eukaryotic structural genomics, *J. Struct. Funct. Genomics 6*, 143−147.
14. Otwinowski, Z., and Minor, W. (1997) Processing of X-ray Diffraction Data Collected in Oscillation Mode, *Methods Enzymol. 276*, 307−326.
15. Vagin, A., and Teplyakov, A. (1997) MOLREP: An Automated Program for Molecular Replacement, *J. Appl. Crystallogr. 30*, 1022−1025.
16. Collaborative Computational Project Number 4 (1994) The CCP4 suite: Programs for protein crystallography, *Acta Crystallogr. D50*, 760−763.
17. Brunger, A. T., Adams, P. D., Clore, G. M., DeLano, W. L., Gros, P., Grosse-Kunstleve, R. W., Jiang, J. S., Kuszewski, J., Nilges, M., Pannu, N. S., Read, R. J., Rice, L. M., Simonson, T., and Warren, G. L. (1998) Crystallography & NMR system: A new software suite for macromolecular structure determination, *Acta Crystallogr. D54* (Part 5), 905−921.
18. Jones, T. A., Zou, J. Y., Cowan, S. W., and Kjeldgaard, M. (1991) Improved methods for building protein models in electron density maps and the location of errors in these models, *Acta Crystallogr. A47* (Part 2), 110−119.
19. McRee, D. E. (1999) XtalView/Xfit: A versatile program for manipulating atomic coordinates and electron density, *J. Struct. Biol. 125*, 156−165.
20. Murshudov, G. N., Vagin, A. A., and Dodson, E. J. (1997) Refinement of macromolecular structures by the maximum-likelihood method, *Acta Crystallogr. D53*, 240−255.
21. Gill, S. C., and von Hippel, P. H. (1989) Calculation of protein extinction coefficients from amino acid sequence data, *Anal. Biochem. 182*, 319−326.
22. Cleland, W. W. (1979) Statistical analysis of enzyme kinetic data, *Methods Enzymol. 63*, 103−138.
23. Wedekind, J. E., Frey, P. A., and Rayment, I. (1995) Three-dimensional structure of galactose-1-phosphate uridylyltransferase from *Escherichia coli* at 1.8 Å resolution, *Biochemistry 34*, 11049−11061.
24. Ruzicka, F. J., Wedekind, J. E., Kim, J., Rayment, I., and Frey, P. A. (1995) Galactose-1-phosphate uridylyltransferase from *Escherichia coli*, a zinc and iron metalloenzyme, *Biochemistry 34*, 5610−5617.
25. Geeganage, S., and Frey, P. A. (1999) Significance of metal ions in galactose-1-phosphate uridylyltransferase: An essential structural zinc and a nonessential structural iron, *Biochemistry 38*, 13398−13406.
26. Wedekind, J. E., Frey, P. A., and Rayment, I. (1996) The structure of nucleotidylated histidine-166 of galactose-1-phosphate uridylyltransferase provides insight into phosphoryl group transfer, *Biochemistry 35*, 11560−11569.
27. Dankert, M., Goncalves, I. R. J., and Recondo, E. (1964) Adenosine diphosphate glucose: Orthophosphate adenylyltransferase in wheat germ, *Biochim. Biophys. Acta 81*, 78−85.
28. Rodriguez-Lopez, M., Baroja-Fernandez, E., Zandueta-Criado, A., and Pozueta-Romero, J. (2000) Adenosine diphosphate glucose pyrophosphatase: A plastidial phosphodiesterase that prevents starch biosynthesis, *Proc. Natl. Acad. Sci. U.S.A. 97*, 8705−8710.
29. Stern, A. I., and Avron, M. (1966) An adenosine 5′-diphosphate ribose:orthophosphate adenylyltransferase from *Euglena gracilis*, *Biochim. Biophys. Acta 118*, 577−591.
30. Carminatti, H., and Cabib, E. (1961) Phosphorolysis of the pyrophosphate bond of some nucleotides, *Biochim. Biophys. Acta 53*, 417−419.
31. Thoden, J. B., Ruzicka, F. J., Frey, P. A., Rayment, I., and Holden, H. M. (1997) Structural analysis of the H166G site-directed mutant of galactose-1-phosphate uridylyltransferase complexed with either UDP-glucose or UDP-galactose: Detailed description of the nucleotide sugar binding site, *Biochemistry 36*, 1212−1222.
32. Ozbun, J. L., Hawker, J. S., Greenberg, E., Lammel, C., and Preiss, J. (1973) Starch synthetase, phosphorylase, ADPglucose pyrophosphorylase, and UDPglucose pyrophosphorylase in developing maize kernels, *Plant Physiol. 51*, 1−5.
33. Geigenberger, P. (2003) Regulation of sucrose to starch conversion in growing potato tubers, *J. Exp. Bot. 54*, 457−465.
34. Baroja-Fernandez, E., Munoz, F. J., Zandueta-Criado, A., Moran-Zorzano, M. T., Viale, A. M., Alonso-Casajus, N., and Pozueta-Romero, J. (2004) Most of ADP x glucose linked to starch biosynthesis occurs outside the chloroplast in source leaves, *Proc. Natl. Acad. Sci. U.S.A. 101*, 13080−13085.
35. Munoz, F. J., Baroja-Fernandez, E., Moran-Zorzano, M. T., Viale, A. M., Etxeberria, E., Alonso-Casajus, N., and Pozueta-Romero, J. (2005) Sucrose synthase controls both intracellular ADP glucose levels and transitory starch biosynthesis in source leaves, *Plant Cell Physiol. 46*, 1366−1376.
36. DeLano, W. L. (2002) *The Pymol User's Manual*, DeLano Scientific, San Carlos, CA.
37. Bond, C. S. (2003) TopDraw: A sketchpad for protein structure topology cartoons, *Bioinformatics 19*, 311−312.
38. Thompson, J. D., Higgins, D. G., and Gibson, T. J. (1994) CLUSTAL W: Improving the sensitivity of progressive multiple sequence alignment through sequence weighting, position-specific gap penalties and weight matrix choice, *Nucleic Acids Res. 22*, 4673−4680.

BI052232M